Carbohydrate Polymers 101 (2014) 961–967

Contents lists available at ScienceDirect

Carbohydrate Polymers

journal homepage: www.elsevier.com/locate/carbpol

Green synthesis of xanthan conformation-based silver nanoparticles: Antibacterial and catalytic application

Wei Xu[a,b], Weiping Jin[a], Liufeng Lin[a], Chunlan Zhang[a], Zhenshun Li[a], Yan Li[a,b], Rong Song[a,b], Bin Li[a,b,*]

[a] College of Food Science and Technology, Huazhong Agriculture University, Wuhan 430070, China
[b] Key Laboratory of Environment Correlative Dietology (Huazhong Agricultural University), Ministry of Education, China

ARTICLE INFO

Article history:
Received 1 September 2013
Received in revised form 8 October 2013
Accepted 13 October 2013
Available online 21 October 2013

Keywords:
Green synthesis
Xanthan gum
Silver nanoparticles
Catalysis
Antibacterial

ABSTRACT

Silver nanoparticles (Ag NPs) were green synthetized using xanthan gum (XG) dissolved in water as reducing and capping agent for the first time. The structure, morphology, and size of Ag NPs in XG aqueous solutions were investigated with UV–vis spectroscopy, transmission electron microscopy and Fourier transform infrared. The results indicated Ag NPs were integrated successfully in the XG matrix and the optical properties and morphology of Ag NPs could be regulated by the synthesis condition. The aggregation of the XG-bonded Ag NPs increased with storage, whereas the size barely changed. The assemble behavior was related to the XG conformation transition of denaturation and renaturation. The one spot formed Ag NPs showed favorable antibacterial effect on *Escherichia coli* and *Staphyloccocus aureus* and excellent catalytic capability of 4-nitrophenol reduction. This work provided a feasible method to detect the biopolymer space structure transition through the intensity of metal nanoparticles labeled on the chain.

1. Introduction

Silver nanoparticle (Ag NPs), one of the noble metal nanoparticles, has attracted extensive attention in the past decades due to its wide application in catalysis, antimicrobial chemical sensing and nanotechnology (Ai, Liu, & Lu, 2009; Narayanan & Sakthivel, 2010; Zhong & Maye, 2001). Chemical reduction is the common method for Ag NPs synthesis (Sharma, Yngard, & Lin, 2009). However, many reductive chemicals used are highly reactive and pose potential environmental and biological risks. Hence, much endeavor has been devoted to hunt for simple, green methods to synthesize Ag NPs. Plant leaf extracts, seed extracts and living organisms have been reported to green synthesis of Ag NPs (Asghari et al., 2012; Bar et al., 2009; Mishra, Kaushik, Sardar, & Sahal, 2013). Recently, studies on synthesis of Ag NPs basis on nature biopolymer have attracted intense attention because of their rich source and biocompatibility (Li et al., 2007; Nadagouda & Varma, 2008). Polysaccharide, pose many hydroxyl groups, has been the potential candidate as a mild reducing agent and a stabilizer for Ag NPs (Chen, Wang, Zhang, & Jin, 2008; Pandey, Goswami, & Nanda, 2013).

Although several kinds of polysaccharide has been used to green synthesis of Ag NPs, including lentinan (Peng, Yang, & Xiong, 2012), agar (Shukla, Singh, Reddy, & Jha, 2012), starch (Vigneshwaran, Nachane, Balasubramanya, & Varadarajan, 2006), locust bean gum (Tagad et al., 2013) and gellan gum (Dhar, Murawala, Shiras, Pokharkar, & Prasad, 2012). However, xanthan gum has not been studied as reducing and capping agent to green form Ag NPs. As we know, many nature polysaccharide poses spatial conformation (Marszalek & Dufrêne, 2012). During the Ag NPs synthesis, heat treatment, electrostatic interaction and binding to polysaccharide chain could exert great influence on its conformation. Accordingly, the polysaccharide also impact on the Ag NPs size and distribution. However, scanty studies have been reported the interaction between Ag NP and polysaccharide during the process of denaturation and renaturation. Lentinan, pose triple helical conformation and denatured into single chains when suffered heat treatment above the midpoint temperature (Tm), had been approved the conformation exerted significant impact on gold nanoparticle synthesis and its distribution (Li, Zhang, Xu, & Zhang, 2011).

Xanthan gum (XG), the extracellular bacterial polysaccharide, is consisted of a β-1,4-linked D-glucose backbone, substituted alternately with a trisaccharide side chain linked to every second glucose residue (Mao, Klinthong, Zeng, & Chen, 2012). It is well established that XG is the ordered 5-fold helix structure in spite of some controversy (Agoub, Smith, Giannouli, Richardson, & Morris, 2007). Green synthesis of Ag NPs reduced by XG was

* Corresponding author at: College of Food Science and Technology, Huazhong Agriculture University, Wuhan 430070, China. Tel.: +86 27 63730040; fax: +86 27 87282966.
E-mail address: libinfood@mail.hzau.edu.cn (B. Li).

0144-8617/$ – see front matter.
http://dx.doi.org/10.1016/j.carbpol.2013.10.032

rarely reported. Additionally, the interactions between XG structure and metal nanoparticles have not been studied before. In this paper, a worth-while endeavor would be using XG as reducing and stabilizing agent for a one step synthesis of Ag NPs. The effect of structure transformation on Ag NPs synthesis was illustrated. The antibacterial effect on pathogenic bacterium and catalytic capability of 4-NP were evaluated. The formed Ag NPs by one spot and free of organic solvent has potential application in biotechnology and biomedicine. Besides, the study also enriches the information of polysaccharide-conjugated metal nanoparticles.

2. Materials and methods

2.1. Materials

Xanthan gum was purchased from Shanghai source Biological Technology Co., Ltd. Silver nitrate ($AgNO_3$), 4-nitro-phenol (4-NP) and sodium borohydride ($NaBH_4$) and other chemical reagents of analytical grade were purchased from commercial sources in China and used without further purification. All the solutions used in the experiments were prepared using ultrapure water through a Millipore (Millipore, Milford, MA, USA) Milli-Q water purification system.

2.2. Synthesis of silver nanoparticles

For synthesis of silver nanoparticles, 0.1 mg of XG was dissolved in 100 ml ultrapure water under constant stirring for dissolution of XG to achieve 0.1% (w/v) solution and $AgNO_3$ was added in the obtained solutions to get the final concentration of 1 mM, 2 mM and 3 mM. The reaction mixtures were incubated for the time period of 12, 24, 36 and 48 h at 60 °C, 80 °C and 100 °C in dark condition with stirring.

2.3. Characterization

UV–visible spectroscopy (UV–vis) was performed using UV spectrophotometer (Shimadzu UV-1700) as a function of reaction time and temperature during the synthesis of Ag NPs. The control was run only 0.1% XG without reduction agent. For transmission electron microscopy (TEM), a drop of XG/Ag colloidal solution was dispensed directly onto a carbon coated copper grid and allowed to dry completely in a vacuum desiccator. Then the pictures of the prepared samples were obtained using a JEOL transmission electron microscope (H-7650, Hitachi, Japan). The Fourier transform infrared (FT-IR) spectra were recorded with a Nicolet Nexus 470 spectrometer with 32 scans and resolution of 4 cm^{-1}.

2.4. In vitro antibacterial assay

The inhibitory zone of XG/Ag nanoparticles were determined by disk diffusion method in the agar medium (Das et al., 2011; Sathishkumar, Sneha, & Yun, 2010). Briefly, the Gram-negative *Escherichia coli* and Gram-positive *Staphyloccocus aureus* were taken as two typical kinds of pathogenic bacteria. The overnight cultured *E. coli* and *S. aureus*, approximately 3.8×10^6 and 4.5×10^5/ml CFU respectively, were added in the 50 ml of agar medium. Filter paper discs (6 mm diameter) were soaked with 15 μL of the XG/Ag nanoparticles solution for 15 min and placed on the inoculated plates. Subsequently, they were incubated at 37 °C for 24 h. The diameters of the inhibition zones were measured by vernier caliper.

2.5. Catalytic reduction of 4-NP

The catalytic 4-NP reduction was carried out in a quartz cuvette and monitored using UV–vis spectroscopy accordingly (Narayanan, Park, & Sakthivel, 2013; Zhang et al., 2011). Firstly, 10 mL of fresh $NaBH_4$ aqueous solution (0.2 M) was mixed with 10 μL of XG/Ag nanoparticle aqueous dispersion. Subsequently, 1 mL of 4-NP solution (2×10^{-4} M) as added into 1 mL above mixture. As a result, the concentration of 4-NP and $NaBH_4$ in the reaction solution was 1×10^{-4} M and 0.1 M, respectively. The reaction was monitored at decided time intervals by measuring the absorbance of nitrophenolate ions at 400 nm.

3. Results and discussion

3.1. Effect of heating time on Ag NPs synthesis

In this study, low cost XG has been used as a reducing and stabilizing agent for Ag NPs synthesis. Silver nanoparticles were formed by the reduction of Ag^+ into Ag^0 with the addition of XG (1 mg ml^{-1}) to the solution of 1 mM $AgNO_3$. The results revealed the synthesis was a slow process at 60 °C (Fig. 1a). The phenomenon of the colorless $AgNO_3$ solution turning into dark brownish yellow color indicated the formation of Ag NPs (Wu, Zhao, Zhang, & Xu, 2012). The absorption spectrum shows no absorption peak until 24 h later. The intense band detected around 420 nm identified as a "surface Plasmon resonance band" and ascribed to the excitation of free electrons in Ag NPs. The shape of the band suggested the uniform dispersal of spherical shape Ag NPs. The increased absorbance as a function of time signifies the enhanced reduction of Ag+ to form Ag NPs. This phenomenon was in accord with the reported literature reduced by other polysaccharide (Raveendran, Fu, & Wallen, 2003). As we know, XG is a polyhydroxylated biopolymer consisting of helical structure. The special inter and intramolecular hydrogen bonding resulted in spatial network formation which acted as templates for Ag NPs synthesis. As the heating time extend, the increased hydroxyl groups on XG chain act as active reduction of Ag^+ to Ag^0. After formed, Ag NPs get embedded and stabilized with the XG matrix.

3.2. Effect of $AgNO_3$ concentration on Ag NPs synthesis

The effect of $AgNO_3$ concentration (1 mM, 2 mM and 3 mM) on synthesis of Ag NPs was investigated with the condition of 0.1% XG, heated 24 h at 60 °C (Fig. 1b). The increased absorption intensity with an increase in $AgNO_3$ concentration shows an enhanced reduction of Ag^+ at higher concentration of $AgNO_3$. Regardless of Ag^+ concentration used, the similar surface plasmon bands are exhibited which reveals that the synthesis of Ag NPs share uniform size and shape in the XG stabilized medium. The increasingly becoming brown of the inset simultaneously proclaims the easy synthesis of Ag NPs in higher Ag^+ concentration.

3.3. Effect of temperature on Ag NPs synthesis

The UV–vis absorption spectra of Ag NPs prepared using different temperature (80 °C, 100 °C) and reaction time (1–4 h), where the $AgNO_3$ and XG concentration was kept constant at 2 mM and 0.1% (w/v), respectively. The results revealed the incubation temperature played an important role in the reduction of Ag NPs. Approximately, 3 h and 2 h was required for Ag NPs formation at 80 °C and 100 °C, respectively (Fig. 2). It is evident that short time was required for Ag NPs synthesis when the temperature was higher. As compared with Fig. 1a, Ag NPs synthesis calls for 24 h at 60 °C, while 2 h at 100 °C. As show in the inset of Fig. 2, the deepening yellow color illustrated the continuous evolution of Ag NPs

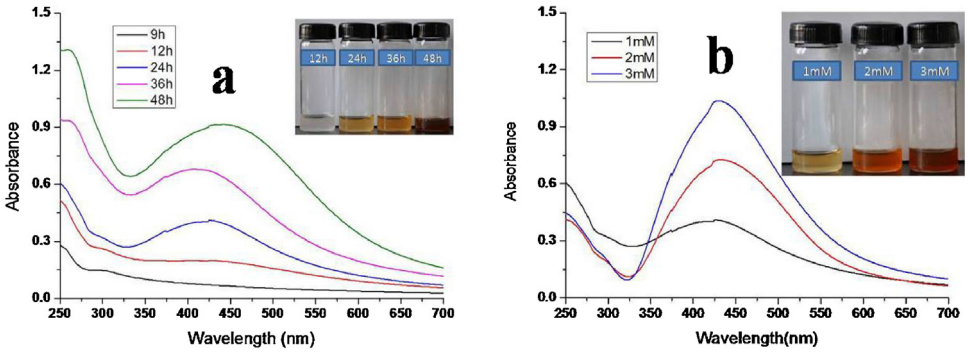

Fig. 1. UV–vis spectra of as Ag NPs a function of reaction time (a) using 1 mM Ag^{1+} and Ag^{1+} concentration (b) for 24 h with 0.1% XG at 60 °C.

formation in XG media. The results coincidently illustrated synthesis of Ag NPs by XG reduction was a slow procedure for low reduction capability and accelerated after denaturation of XG. However, the higher stability of XG/Ag nanoparticle solution testified XG structure matrix acted as a benign template for Ag crystal growth.

3.4. Morphology evolution of Ag NPs synthesis

Based on the color changes of the solutions with different heating time, the different sizes of Ag NPs reduced by XG were confirmed by TEM. The gradual size evolution of Ag NPs is clearly demonstrated in Fig. 3. The Ag NPs were not synthesized until the mixtures were heated for 12 h. The system could not provide enough reduce capability for Ag NPs synthesis until the XG helical denatured and much more hydroxyls were exposed due to thermal treatment. Herein, scarce Ag NPs were formed within the timescale of 12 h. With the heat time extending, much more Ag NPs were synthesized and they all exhibited inerratic spherical appearance. More interestingly, the size of Ag NPs was in a time-dependent manner. When processed at 60 °C for 12 h, the formed Ag NPs sizes existed relatively wide distributing with a diameter of 10–31 nm. After 24 h reduction, spherical Ag NPs with a diameter of 5–20 nm were predominant. While the sizes substantially aggregated as reduced for 36 h and 48 h and turned to be inhomogenous. This phenomenon may relate with the structure of XG matrix. As suffered heat process, the synthesis of helica XG regularly disengaged and exposed the molecular chain. The external hydroxyl groups exert the reduction effect. The disengaged degree determined the renaturation behavior. The steric hindrance of XG deterred the renaturation at low disengaged degree when suffered shorted heat process. On the contrary, renaturation behavior was favor to size aggregation. As Fig. 3 shown, moderate thermal time made Ag NPs favorable size and distribution.

As shown in Fig. 4, the size of the Ag NPs became more uniform as treated at 100 °C. Well related with Fig. 3, the amount of Ag NPs quickly improved with an increase in reaction time, further confirming the occurrence of rapid reduction at higher temperature. It was noted that the temperature exerted a positive effect on the size and distribution. As Fig. 4 shown, the synthetic Ag NPs was slightly aggregated and exhibited size of 8–40 nm after a 2 h reduction at 80 °C. While the size demonstrated better distribution raged from 8 nm to 25 nm in the later 2 h. Compared with treatment at 80 °C, the XG stabled Ag NPs shared a narrow distribution with size of 5–20 nm. Especially after 3 h thermal treatment, the spherical Ag NPs size with a diameter of 5–15 nm were observed. It was suggested that the thermal treatment time also played an indispensable role in the formation of spherical but not the only one.

3.5. FT-IR spectra of Ag NPs bonded-XG

FTIR spectra were studied for identifying the possible groups in XG that were responsible for synthesis and capped of Ag NPs (Fig. 5). The FTIR spectra of Ag NPs bonded-XG formed in different condition has the coincident absorption peak with that of XG, including the characteristic absorption peak of mannopyranose (897 cm^{-1}) (Xin et al., 2012). The band at 3415–3450 cm^{-1} was due to hydroxyl (—OH) stretch. The peak at 1732 cm^{-1} is assigned to the stretching vibration of C=O groups in acetyl group (Deng et al., 2011). It was obvious that the robust bands at 1384 cm^{-1} and 1053 cm^{-1} arise from the NO_3^- addition. Compared with the hydroxyl stretch of XG, the peak of Ag NPs bonded-XG shifts to low wave number, illustrating that intermolecular interaction between Ag NPs bonded XG was weaker than that of XG. The results were consistent with the XG conformation transition of denaturation and renaturation during Ag NPs synthesis. The arresting phenomenon suggests the exposed hydroxyl groups play key role an in reducing and stabilizing Ag NPs.

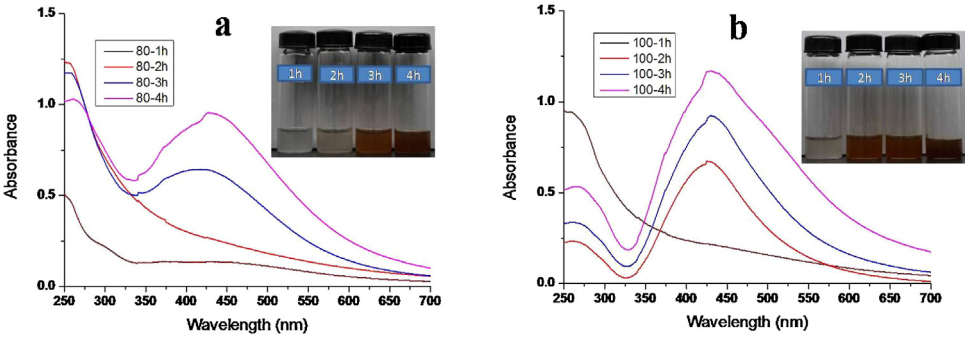

Fig. 2. UV–vis absorption spectra of Ag NPs prepared 80 °C (a) and 100 °C (b) with 1 mM Ag^{1+}. (For interpretation of the references to color in text, the reader is referred to the web version of the article.)

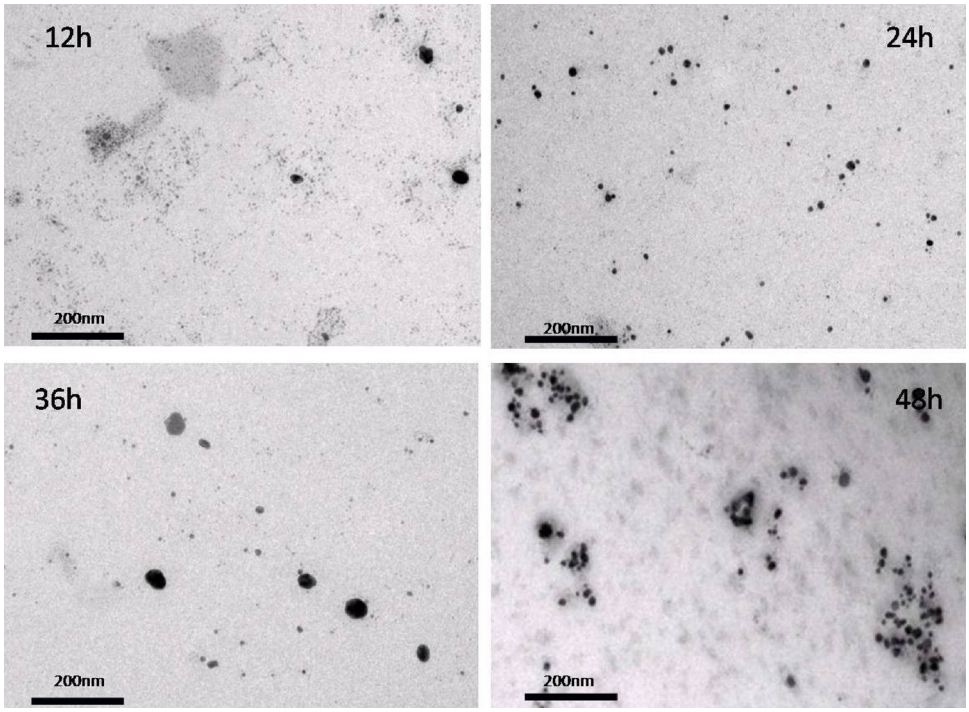

Fig. 3. TEM images of Ag NPs synthesized at different time using 1 mM Ag^{1+} and 0.1% XG at 60 °C.

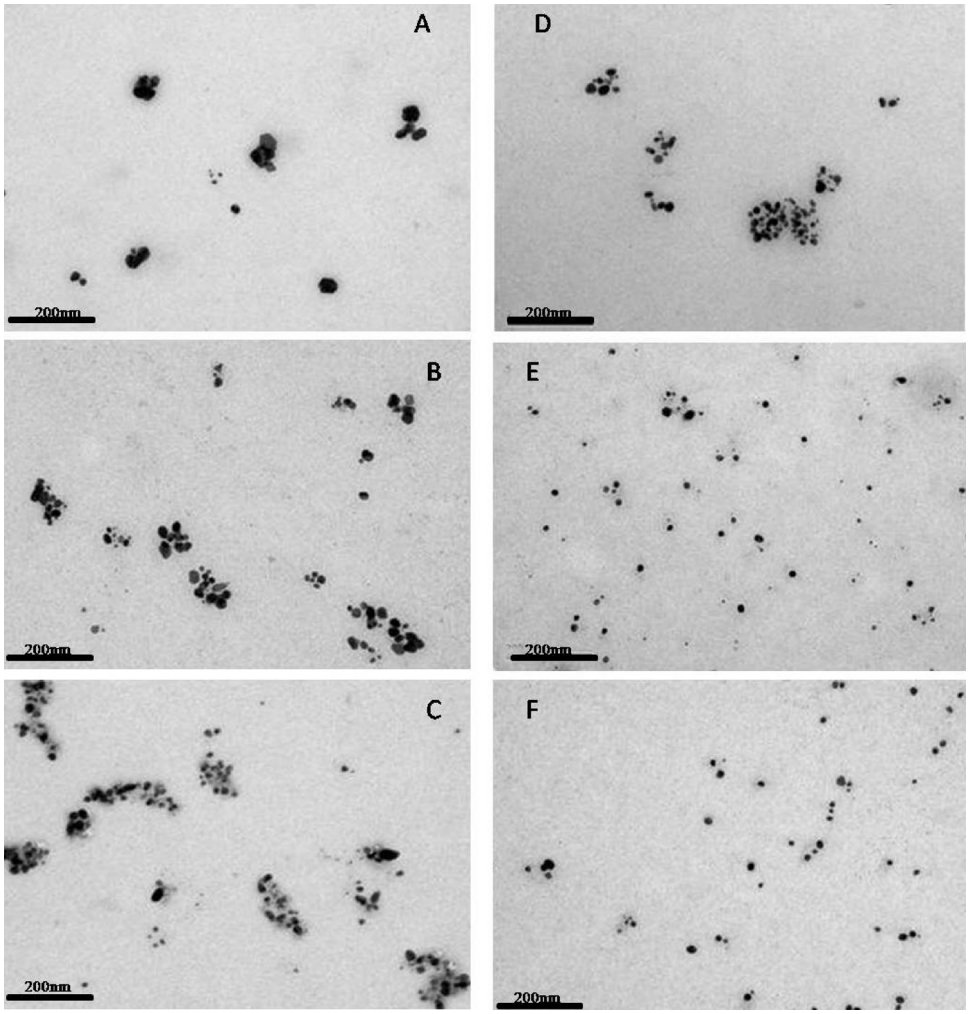

Fig. 4. TEM images of Ag NPs synthesized at 80 °C for 2 h (A), 3 h (B), 4 h (C) and 100 °C for 2 h (D), 3 h (E), 4 h (F) with 1 mM Ag^{1+}.

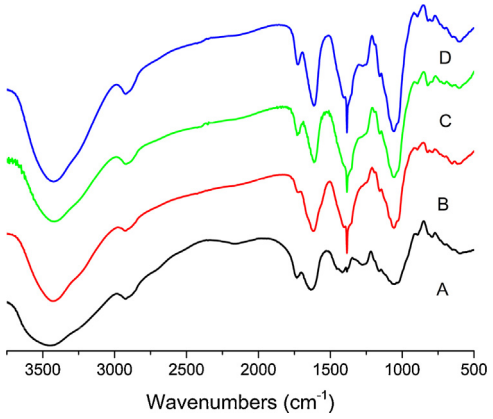

Fig. 5. FTIR spectra of XG (A) and Ag NPs synthesized at 60 °C for 24 h (B), 80 °C for 2 h (C), 100 °C for 1 h (D) with 2 mM Ag^{1+}.

3.6. Xanthan conformation-based Ag NPs synthesis

On the basis of aforementioned results, we proposed a tentative model to illustrate the binding of the Ag NPs to helical and dispersion in XG solution as shown in Fig. 6. Although exist some controversy, the ordered XG structure is established as a 5-fold helix. At the temperature above Tm (60 °C), the denaturation occurs and XG exists in a disordered coil state, while exhibited a rigid, ordered structure during the cooling treatment (Kool et al., 2013). During the denaturation, the exposed oxhydryls endow XG reduction ability to Ag NPs synthesis. Through the high electronegativity bind to XG chain, the formed Ag NPs were prevented from aggregation and demonstrated good dispersion (Fig. 6a). However, the distance between Ag NPs decreased during XG renaturation due to intra- and inter-molecule hydrogen bonds after 1-week storage (Fig. 6b). But the helical structure of XG was found difficult to reform as before due to the Ag NPs steric hindrance. As previously reported, the Ag NPs did not cluster in the dense arrangement and the size almost maintained stable (Li et al., 2011). After 4-week storage (4 °C), the denatured single chains re-associated into loose several-fold helix and lager micro-rods were formed as the helix increased. Ag NPs were found to bind to the chain surface and entrap in the hydrophobic cavity of the folded helix (Fig. 6c).

3.7. Antibacterial activity of Ag NPs

The antibacterial activity of XG/Ag NPs was analyzed by disk diffusion. The clear inhibitory zone appeared around XG/Ag NPs disk after incubation about 24 h, suggesting that XG/Ag NPs completely inhibited *E. coli* and *S. aureus* growth (Fig. 7). As previous study, Ag NPs exerted an anti-microbial effect on Gram-negative bacteria (Guzman, Dille, & Godet, 2012), including coli (Fig. 7A). It was believed that Ag NPs interacted with the material of bacterial cell wall, which further caused the formation of irregular-shaped pits in the outer membrane and changed membrane permeability. A hot favorite was lipopolysaccharide (LPS) molecules, which provide an effective permeability barrier (Li et al., 2010). While it was worth noting that XG/Ag NPs had a more severe antibacterial effect from the zone of inhibition. The zones of inhibition for *S. aureus* growth were 12.3 mm, 12.1 mm and 12.6 mm, while were 9.7 mm, 9.8 mm and 10.7 mm for *E. coli* respectively as the Ag NPs were synthesized at 60 °C for 24 h, 80 °C for 3 h and 100 °C for 3 h accordingly. The antibacterial ability was as high as that of silver nanoparticles impregnated with antibiotics (Geoprincy, Saravanan, Gandhi, & Renganathan, 2011). It was interesting that the formed XG/Ag NPs displayed different inhibition effect. For *S. aureus*, there was no significant difference between the different formed Ag NPs. However, the Ag NPs synthesized at high temperature showed more severe inhibition on *E. coli*. This phenomenon was resulted from different concentration and size of the Ag NPs (Xiu, Zhang, Puppala, Colvin, & Alvarez, 2012). The Ag NPs amount and morphology determined the inhibition of *E. coli.* Nevertheless, the Antibacterial effect of *S. aureus* may depend on concentration of Ag NPs. On the other hand, the mechanism of inhibitory action of Ag NPs was not just the interacted with the bacterial cell wall, but binds to functional groups of proteins and DNA as well (Marambio-Jones & Hoek, 2010).

3.8. Catalytic properties of Ag NPs

Catalytic behavior of the as-prepared XG/Ag NPs was examined through the model reaction of 4-NP reduced by $NaBH_4$. The plots of $\ln(C_t/C_0)$ *versus* time with varied formed XG/Ag NPs were demonstrated in Fig. 8. Obviously, all curves displayed the first-order kinetics (All R^2 of the fitted lines are more than 0.98). The corresponding apparent rate constants k_{app} could be obtained by fitting these curves. It is interesting to note that of Ag NPs k_{app} was determined by the synthesis conditions. Much more Ag NPs were synthesized as higher concentration of silver nitrate provided

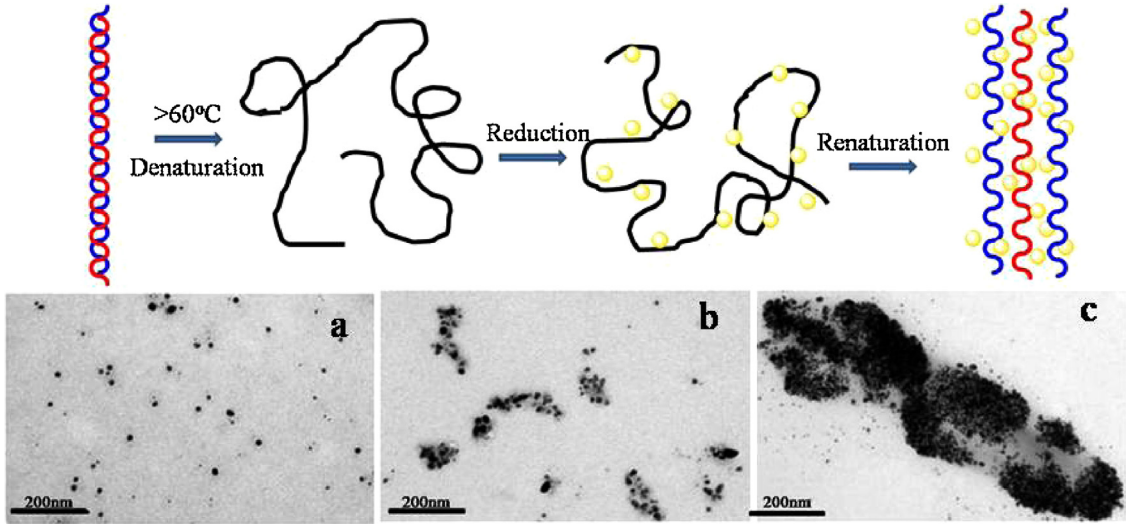

Fig. 6. The scheme of synthesis and dispersion of fresh prepared (a), 1 week (b) and 4 week stored (c) of Ag NPs.

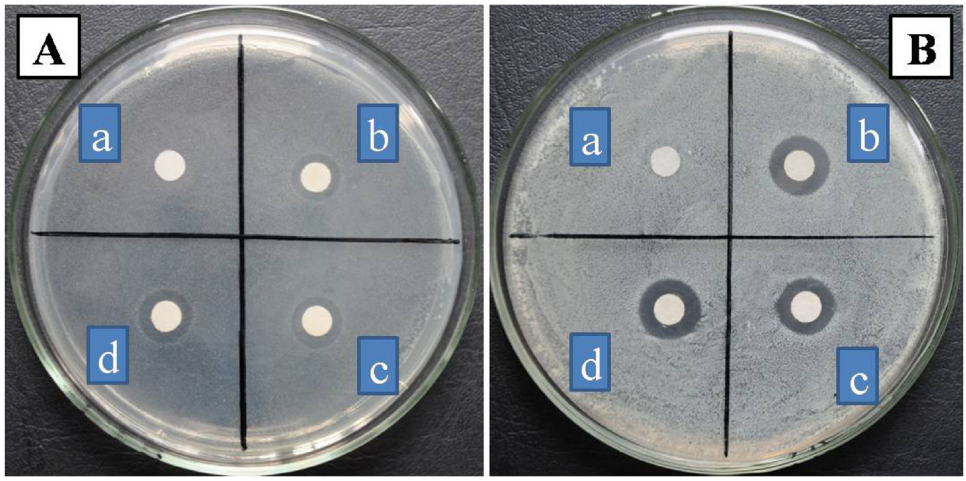

Fig. 7. Zone of inhibition produced by Ag nanoparticles formed at 60 °C for 24 h (b), 80 °C for 2 h (c) and 100 °C (d) for 2 h with *Escherichia coli* (A) and *Staphyloccocus aureus* (B).

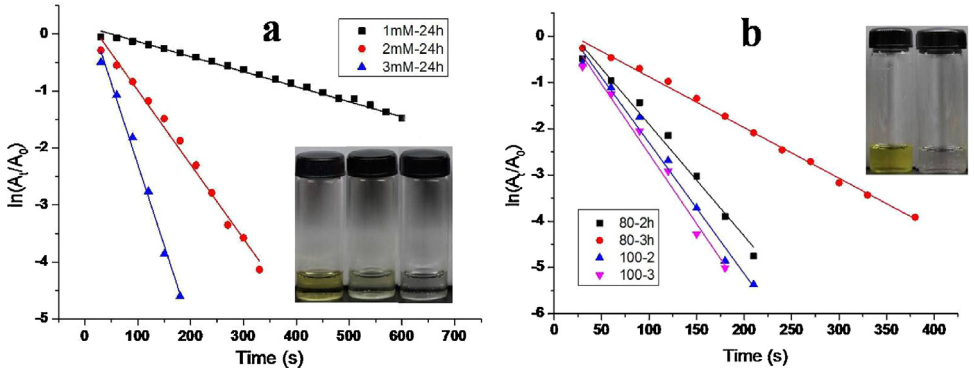

Fig. 8. The relationship between $\ln(C_t/C_0)$ and reaction time with Ag NPs synthesized at different Ag^{1+} concentration at 60 °C (a) and different temperature using 2 mM Ag^{1+} as XG was 0.1%.

(Fig. 1b). As Fig. 8a shown, the k_{app} were 0.00264 s^{-1}, 0.013 s^{-1} and 0.02842 s^{-1} respectively as Ag NPs were formed at 60 °C for 24 h with silver nitrate concentration of 1 mM, 2 mM and 3 mM accordingly. Comparatively, Ag NP formed at 80 °C and 100 °C shared higher k_{app} (Fig. 8b). The k_{app} were 0.02413 s^{-1}, 0.01097 s^{-1}, 0.02827 s^{-1} and 0.03018 s^{-1} as Ag NPs synthesized at 80 °C for 2 h, 3 h and at 100 °C for 2 h, 3 h, respectively. However, the catalytic action cloud be completed with 10 min in all case as the inset shown. The apparent rate constants were about 2–4 folded for silver nanoparticles formed by aromatic nitro compounds and much high for silver-deposited magnetic nanoparticles (1.5×10^{-2} S^{-1}) (Kundu, Mandal, Ghosh, & Pal, 2004; Shin, Choi, Park, Jang, & Kim, 2009). As the previous study, k_{app} mainly depend on the total surface S of Ag NPs (Wunder, Polzer, Lu, Mei, & Ballauff, 2010). It was well related with the Ag NPs size and distribution in Fig. 4. The large specific surface area of Ag NPa is favorable for the diffusion of 4-NP and makes it high reduction.

4. Conclusions

Water dispersible silver nanoparticles with size of 5–40 nm were synthesized in XG aqueous solution. The results of spectral absorption and TEM revealed that the Ag NPs were formed affected by the temperature, silver nitrate concentration and heating time. XG/Ag NPs shared good dispersion by the strong electrostatic interactions between the XG and the Ag NPs. Moreover, the Ag NPs aggregation behavior was related to the conformation transition of the XG between the helix and random coil in the solution. A feasible method to detect the space structure transition of biopolymer was established based on the intensity of metal nanoparticles labeled on the chain. The excellent antibacterial effect and catalytic capability of Ag NPs showed great potential in the biological field *via* the green pathway.

Acknowledgments

This work was financially supported by the National Natural Science Foundation of China (Grant Nos. 31071607 and 31301451). The authors greatly thank colleagues of Key Laboratory of Environment Correlative Dietology of Huazhong Agricultural University for offering many conveniences.

References

Agoub, A., Smith, A. M., Giannouli, P., Richardson, R., & Morris, E. (2007). "Melt-in-the-mouth" gels from mixtures of xanthan and konjac glucomannan under acidic conditions: A rheological and calorimetric study of the mechanism of synergistic gelation. *Carbohydrate Polymers*, *69*(4), 713–724.

Ai, K., Liu, Y., & Lu, L. (2009). Hydrogen-bonding recognition-induced color change of gold nanoparticles for visual detection of melamine in raw milk and infant formula. *Journal of the American Chemical Society*, *131*(27), 9496–9497.

Asghari, S., Johari, S. A., Lee, J. H., Kim, Y. S., Jeon, Y. B., Choi, H. J., et al. (2012). Toxicity of various silver nanoparticles compared to silver ions in *Daphnia magna*. *Journal of Nanobiotechnology*, *10*(1), 14.

Bar, H., Bhui, D. K., Sahoo, G. P., Sarkar, P., Pyne, S., & Misra, A. (2009). Green synthesis of silver nanoparticles using seed extract of *Jatropha curcas*. *Colloids and Surfaces A: Physicochemical and Engineering Aspects*, *348*(1), 212–216.

Chen, J., Wang, J., Zhang, X., & Jin, Y. (2008). Microwave-assisted green synthesis of silver nanoparticles by carboxymethyl cellulose sodium and silver nitrate. *Materials Chemistry and Physics*, *108*(2), 421–424.

Das, M. R., Sarma, R. K., Saikia, R., Kale, V. S., Shelke, M. V., & Sengupta, P. (2011). Synthesis of silver nanoparticles in an aqueous suspension of graphene oxide sheets and its antimicrobial activity. *Colloids and Surfaces B: Biointerfaces*, *83*(1), 16–22.

Deng, H., Li, X., Ding, B., Du, Y., Li, G., Yang, J., et al. (2011). Fabrication of polymer/layered silicate intercalated nanofibrous mats and their bacterial inhibition activity. *Carbohydrate Polymers*, *83*(2), 973–978.

Dhar, S., Murawala, P., Shiras, A., Pokharkar, V., & Prasad, B. (2012). Gellan gum capped silver nanoparticle dispersions and hydrogels: Cytotoxicity and in vitro diffusion studies. *Nanoscale*, *4*(2), 563–567.

Guzman, M., Dille, J., & Godet, S. (2012). Synthesis and antibacterial activity of silver nanoparticles against Gram-positive and Gram-negative bacteria. *Nanomedicine: Nanotechnology, Biology and Medicine*, *8*(1), 37–45.

Geoprincy, G., Saravanan, P., Gandhi, N. N., & Renganathan, S. (2011). A novel approach for studying the combined antimicrobial effects of silver nanoparticles and antibiotics through agar over layer method and disk diffusion method. *Digest Journal of Nanomaterials and Biostructures*, *6*(4), 1557–1565.

Kool, M. M., Schols, H. A., Delahaije, R. J., Sworn, G., Wierenga, P. A., & Gruppen, H. (2013). The influence of the primary and secondary xanthan structure on the enzymatic hydrolysis of the xanthan backbone. *Carbohydrate Polymers*, *97*(2), 368–375.

Kundu, S., Mandal, M., Ghosh, S. K., & Pal, T. (2004). Photochemical deposition of SERS active silver nanoparticles on silica gel and their application as catalysts for the reduction of aromatic nitro compounds. *Journal of Colloid and Interface Science*, *272*(1), 134–144.

Li, S., Shen, Y., Xie, A., Yu, X., Qiu, L., Zhang, L., et al. (2007). Green synthesis of silver nanoparticles using *Capsicum annuum* L. extract. *Green Chemistry*, *9*(8), 852–858.

Li, S., Zhang, Y., Xu, X., & Zhang, L. (2011). Triple helical polysaccharide-induced good dispersion of silver nanoparticles in water. *Biomacromolecules*, *12*(8), 2864–2871.

Li, W. R., Xie, X. B., Shi, Q. S., Zeng, H. Y., You-Sheng, O. Y., & Chen, Y. B. (2010). Antibacterial activity and mechanism of silver nanoparticles on *Escherichia coli*. *Applied Microbiology and Biotechnology*, *85*(4), 1115–1122.

Mao, C. F., Klinthong, W., Zeng, Y. C., & Chen, C. H. (2012). On the interaction between konjac glucomannan and xanthan in mixed gels: An analysis based on the cascade model. *Carbohydrate Polymers*, *89*(1), 98–103.

Marambio-Jones, C., & Hoek, E. M. (2010). A review of the antibacterial effects of silver nanomaterials and potential implications for human health and the environment. *Journal of Nanoparticle Research*, *12*(5), 1531–1551.

Marszalek, P. E., & Dufrêne, Y. F. (2012). Stretching single polysaccharides and proteins using atomic force microscopy. *Chemical Society Reviews*, *41*(9), 3523–3534.

Mishra, A., Kaushik, N. K., Sardar, M., & Sahal, D. (2013). Evaluation of antiplasmodial activity of green synthesized silver nanoparticles. *Colloids and Surfaces B: Biointerfaces*, *111c*, 713–718.

Nadagouda, M. N., & Varma, R. S. (2008). Green synthesis of silver and palladium nanoparticles at room temperature using coffee and tea extract. *Green Chemistry*, *10*(8), 859–862.

Narayanan, K. B., Park, H. H., & Sakthivel, N. (2013). Extracellular synthesis of mycogenic silver nanoparticles by *Cylindrocladium floridanum* and its homogeneous catalytic degradation of 4-nitrophenol. *Spectrochimica Acta Part A: Molecular and Biomolecular Spectroscopy*, *116*, 485–490.

Narayanan, K. B., & Sakthivel, N. (2010). Biological synthesis of metal nanoparticles by microbes. *Advances in Colloid and Interface Science*, *156*(1), 1–13.

Pandey, S., Goswami, G. K., & Nanda, K. K. (2013). Green synthesis of polysaccharide/gold nanoparticle nanocomposite: An efficient ammonia sensor. *Carbohydrate Polymers*, *94*(1), 229–234.

Peng, H., Yang, A., & Xiong, J. (2012). Green, microwave-assisted synthesis of silver nanoparticles using bamboo hemicelluloses and glucose in an aqueous medium. *Carbohydrate Polymers*, *91*(1), 348–355.

Raveendran, P., Fu, J., & Wallen, S. L. (2003). Completely "green" synthesis and stabilization of metal nanoparticles. *Journal of the American Chemical Society*, *125*(46), 13940–13941.

Sathishkumar, M., Sneha, K., & Yun, Y.-S. (2010). Immobilization of silver nanoparticles synthesized using Curcuma longa tuber powder and extract on cotton cloth for bactericidal activity. *Bioresour Technol*, *101*(20), 7958–7965.

Sharma, V. K., Yngard, R. A., & Lin, Y. (2009). Silver nanoparticles: Green synthesis and their antimicrobial activities. *Advances in Colloid and Interface Science*, *145*(1), 83–96.

Shin, K. S., Choi, J.-Y., Park, C. S., Jang, H. J., & Kim, K. (2009). Facile synthesis and catalytic application of silver-deposited magnetic nanoparticles. *Catalysis Letters*, *133*(1–2), 1–7.

Shukla, M. K., Singh, R. P., Reddy, C., & Jha, B. (2012). Synthesis and characterization of agar-based silver nanoparticles and nanocomposite film with antibacterial applications. *Bioresource Technology*, *107*, 295–300.

Tagad, C., Dugasani, S., Aiyer, R., Park, S., Kulkarni, A., & Sabharwal, S. (2013). Green synthesis of silver nanoparticles and their application for the development of optical fiber based hydrogen peroxide sensor. *Sensors and Actuators B: Chemical*, *183*, 144–149.

Vigneshwaran, N., Nachane, R., Balasubramanya, R., & Varadarajan, P. (2006). A novel one-pot 'green'synthesis of stable silver nanoparticles using soluble starch. *Carbohydrate Research*, *341*(12), 2012–2018.

Wu, J., Zhao, N., Zhang, X., & Xu, J. (2012). Cellulose/silver nanoparticles composite microspheres: Eco-friendly synthesis and catalytic application. *Cellulose*, *19*(4), 1239–1249.

Wunder, S., Polzer, F., Lu, Y., Mei, Y., & Ballauff, M. (2010). Kinetic analysis of catalytic reduction of 4-nitrophenol by metallic nanoparticles immobilized in spherical polyelectrolyte brushes. *Journal of Physical Chemistry C*, *114*(19), 8814–8820.

Xin, S., Li, Y., Li, W., Du, J., Huang, R., Du, Y., et al. (2012). Carboxymethyl chitin/organic rectorite composites based nanofibrous mats and their cell compatibility. *Carbohydrate Polymers*, *90*(2), 1069–1074.

Xiu, Z.-m., Zhang, Q.-b., Puppala, H. L., Colvin, V. L., & Alvarez, P. J. (2012). Negligible particle-specific antibacterial activity of silver nanoparticles. *Nano Letters*, *12*(8), 4271–4275.

Zhang, P., Shao, C., Zhang, Z., Zhang, M., Mu, J., Guo, Z., et al. (2011). In situ assembly of well-dispersed Ag nanoparticles (AgNPs) on electrospun carbon nanofibers (CNFs) for catalytic reduction of 4-nitrophenol. *Nanoscale*, *3*(8), 3357–3363.

Zhong, C.-J., & Maye, M. M. (2001). Core–shell assembled nanoparticles as catalysts. *Advanced Materials*, *13*(19), 1507–1511.